Lattice Boltzmann Simulations of Binary Fluid Flow through Porous Media
Author(s): Jonas Tölke, Manfred Krafczyk, Manuel Schulz and Ernst Rank
Source: *Philosophical Transactions: Mathematical, Physical and Engineering Sciences*, Vol. 360, No. 1792, Discrete Modelling and Simulation of Fluid Dynamics (Mar. 15, 2002), pp. 535-545
Published by: Royal Society
Stable URL: http://www.jstor.org/stable/3066331
Accessed: 24-08-2017 00:52 UTC

10.1098/rsta.2001.0944

THE ROYAL SOCIETY

Lattice Boltzmann simulations of binary fluid flow through porous media

BY JONAS TÖLKE[1], MANFRED KRAFCZYK[1], MANUEL SCHULZ[2] AND ERNST RANK[2]

[1]*Institut für Computeranwendungen im Bauwesen, Fachbereich Bauingenieurwesen, Technische Universität Braunschweig, Pockelstraße 3, D-38106 Braunschweig, Germany* (toelke@inf.bauwesen.tu-muenchen.de)

[2]*Lehrstuhl für Bauinformatik, Fakultät für Bauingenieur- und Vermessungswesen, Technische Universität München, Arcisstraße 21, D-80290 München, Germany*

Published online 12 February 2002

The lattice Boltzmann equation is often advocated as a simulation tool that is particularly effective for complex fluids such as multiphase and multicomponent flows through porous media. We construct a three-dimensional 19 velocity lattice Boltzmann model for immiscible binary fluids with variable viscosities and density ratio based on the model proposed by Gunstensen. The model is tested for the following binary fluid flow problems: a stationary planar interface among two fluids; channel flow of immiscible binary fluids; the Laplace problem; and a rising bubble. The results agree well with semi-analytic results in a range of the Eötvös, Morton and Reynolds number. We also present preliminary simulation results for two large-scale realistic applications: the flow of an air–water mixture in a waste-water batch reactor and the saturation hysteresis effect in soil flow. We discuss some limitations of the lattice Boltzmann method in the simulation of realistic and difficult multiphase problems.

Keywords: Boltzmann method; multiphase flow; porous media

1. Introduction

In the last decade there have been a number of lattice Boltzmann models proposed for complex flows of multiphase and multicomponent fluids (see, for example, Chen & Doolen (1998) and references cited therein), and most of these lattice Boltzmann models are based upon the Bhatnagar–Gross–Krook (BGK) model (Bhatnagar *et al.* 1954). So far by and large the numerical results of multiphase and multicomponent fluids obtained by using the lattice Boltzmann models are qualitative in nature.

In this paper we intend to investigate the applicability of the lattice Boltzmann model for immiscible binary fluids to realistic industrial problems. We first discuss the Rothman–Keller model (Rothman & Keller 1988) and its variations. We then introduce a three-dimensional 19 velocity (D3Q19) lattice Boltzmann model for immiscible binary fluids with variable viscosities and density ratio. We focus our attention on the improvement of the 'recolouring' algorithm, which mimics the separation in the immiscible binary mixture. We propose an improved 'recolouring' algorithm which

minimizes spurious currents in interface regions. We validate the model through a set of tests for which semi-analytic solutions are available. Finally, we present preliminary simulation results for two-phase flow in a waste-water batch reactor and the direct simulation of saturation hysteresis effects in soil flow. Through the realistic applications, we demonstrate the capability of the lattice Boltzmann model for immiscible fluids to quantitatively simulate the behaviour of complex fluids in porous media.

2. D3Q19 lattice Boltzmann equation (LBE) model for immiscible binary fluids

The first lattice-gas model for immiscible binary fluids was proposed by Rothman & Keller (1988) and the equivalent lattice BGK (LBGK) model was proposed by Gunstensen & Rothman (1991). Grunau *et al.* (1993) modified the model for binary fluids with different density ratios and viscosities on a triangular lattice in two dimensions. Here we shall construct a three-dimensional 19 velocity lattice Boltzmann model (D3Q19) for immiscible binary fluids based upon the existing models.

Let f_a^{r}, f_a^{b}, and f_a denote the particle distribution functions of a red fluid, a blue fluid, and their mixture, respectively. The macroscopic variables are

$$\rho^{\mathrm{r}} = \sum_a f_a^{\mathrm{r}}, \qquad \rho^{\mathrm{b}} = \sum_a f_a^{\mathrm{b}}, \qquad \rho = \rho^{\mathrm{r}} + \rho^{\mathrm{b}}, \qquad \rho \boldsymbol{u} = \sum_a \boldsymbol{\xi}_a (f_a^{\mathrm{r}} + f_a^{\mathrm{b}}). \tag{2.1}$$

The order parameter in the system of a binary mixture is

$$\Phi = \frac{\rho^{\mathrm{r}} - \rho^{\mathrm{b}}}{\rho^{\mathrm{r}} + \rho^{\mathrm{b}}}. \tag{2.2}$$

The values of the order parameter $\Phi = 1$, -1 and 0 correspond to a purely red fluid, a purely blue fluid, and the interface, respectively. The lattice Boltzmann equations for both the red and blue fluids are

$$f_a^{\mathrm{l}}(t + \Delta t, \boldsymbol{x} + \boldsymbol{\xi}_a \Delta t) = f_a^{\mathrm{l}}(t, \boldsymbol{x}) + \Delta t \Omega_a^{\mathrm{l}}(t, \boldsymbol{x}), \quad \mathrm{l} = \mathrm{r}, \mathrm{b}, \quad a = 0, \ldots, N-1, \tag{2.3}$$

where superscript 'l' indicates either the red or blue fluid, and $\Omega_a^{\mathrm{l}}(t, \boldsymbol{x})$ is the collision operator. The collision operator is made of three parts:

$$\Omega_a^{\mathrm{l}} = \Omega 3_a^{\mathrm{l}} \{\Omega 1_a^{\mathrm{l}} + \Omega 2_a^{\mathrm{l}}\}, \tag{2.4}$$

where

$$\Omega 1_a^{\mathrm{l}} = -\frac{1}{\tau^{\mathrm{l}}}(f_a^{\mathrm{l}} - f_a^{\mathrm{l},(0)})$$

is the usual single relaxation time operator, $\Omega 2_a^{\mathrm{l}}$ is the operator responsible for the generation of surface tension, and $\Omega 3_a^{\mathrm{l}}$ represents the 'recolouring', which mimics the separation mechanism. The distributions after applying the first, second and third operator are denoted by $f_a^{\mathrm{l}\prime}$, $f_a^{\mathrm{l}\prime\prime}$ and $f_a^{\mathrm{l}\prime\prime\prime}$, respectively.

(*a*) *Equilibrium distribution functions*

The equilibrium distribution functions are given by Schelkle (1996):

$$f_a^{(0)} = \rho\left(\alpha^{\mathrm{l}} - \frac{1}{2c^2}\boldsymbol{u}^2\right), \qquad a = 0, \tag{2.5}$$

$$f_a^{(0)} = \rho\left(\frac{1}{18}(1-\alpha^{\mathrm{l}}) + \frac{1}{6c^2}(\boldsymbol{\xi}_a\cdot\boldsymbol{u}) + \frac{1}{4c^4}(\boldsymbol{\xi}_a\cdot\boldsymbol{u})^2 - \frac{1}{12c^2}\boldsymbol{u}^2\right), \quad a = 1,\ldots,6, \tag{2.6}$$

$$f_a^{(0)} = \rho\left(\frac{1}{18}(1-\alpha^{\mathrm{l}}) + \frac{1}{12c^2}(\boldsymbol{\xi}_a\cdot\boldsymbol{u}) + \frac{1}{8c^4}(\boldsymbol{\xi}_a\cdot\boldsymbol{u})^2 - \frac{1}{24c^2}\boldsymbol{u}^2\right), \quad a = 7,\ldots,18, \tag{2.7}$$

where α^{l} is an adjustable parameter, and c is an arbitrary molecular velocity which is typically set to unity. The parameter α^{l} determines the sound speed $c_{\mathrm{s}}^{\mathrm{l}}$ in fluids:

$$c_{\mathrm{s}}^{\mathrm{l}2} = c^2\tfrac{5}{9}(1-\alpha^{\mathrm{l}}). \tag{2.8}$$

The density ratio of the two phases is defined by the ideal gas law and the balance of the hydrodynamic pressure at interfaces:

$$\frac{\rho^{\mathrm{r}}}{\rho^{\mathrm{b}}} = \frac{c_{\mathrm{s}}^{\mathrm{b}2}}{c_{\mathrm{s}}^{\mathrm{r}2}}. \tag{2.9}$$

If the viscosities of the two fluids are not equal, we use a linear interpolation for the relaxation parameter τ in the vicinity of the interface:

$$\tau = \tfrac{1}{2}(1+\Phi)\tau^{\mathrm{r}} + \tfrac{1}{2}(1-\Phi)\tau^{\mathrm{b}}. \tag{2.10}$$

(*b*) *Surface tension generation*

For the generation of surface tension, the distributions are modified in the following way:

$$\Omega 2_a^{\mathrm{l}} = A|\boldsymbol{C}|\left(\frac{(\boldsymbol{e}_a\cdot\boldsymbol{C})^2}{\boldsymbol{C}^2} - \frac{5}{9}\right). \tag{2.11}$$

The colour gradient C_α is computed from

$$C_\alpha = \frac{1}{\Delta t c}\sum_a e_{a\alpha}(\rho^{\mathrm{r}}(t,\boldsymbol{x}+\Delta t\boldsymbol{\xi}_a) - \rho^{\mathrm{b}}(t,\boldsymbol{x}+\Delta t\boldsymbol{\xi}_a)), \tag{2.12}$$

where the free parameter A is proportional to the surface tension σ and $\boldsymbol{e}_a = \boldsymbol{\xi}_{ac}$. Note that the same collision operator is applied for both fluids. If the viscosities of the two fluids are equal, then the value of the surface tension can be approximately predicted by the following formula:

$$\sigma = \frac{1}{\Delta t c}120A\tau(\rho^{\mathrm{r}} + \rho^{\mathrm{b}}). \tag{2.13}$$

(c) Recolouring algorithm

The recolouring collision step redistributes $f_a^{\mathrm{l}\prime\prime}$ to achieve the separation of the two fluids. It is represented by the following maximization problem (Gunstensen & Rothman 1991):

$$\max_{j^{\mathrm{r}\prime\prime\prime}} \boldsymbol{C} \cdot \boldsymbol{j}^{\mathrm{r}\prime\prime\prime} = \max_{f_a^{\mathrm{r}\prime\prime\prime}} \boldsymbol{C} \cdot \sum_a \boldsymbol{e}_a f_a^{\mathrm{r}\prime\prime\prime}. \tag{2.14}$$

Obviously, the recolouring collision must conserve the masses of the two fluids individually, and the momentum and the pressure tensor of the mixture as well. The conservation constraints are expressed as

$$\sum_a f_a^{\mathrm{l}\prime\prime\prime} = \sum_a f_a^{\mathrm{l}\prime\prime} = \rho^{\mathrm{l}}, \tag{2.15}$$

$$f_a^{\mathrm{r}\prime\prime} + f_a^{\mathrm{b}\prime\prime} = f_a^{\mathrm{r}\prime\prime\prime} + f_a^{\mathrm{b}\prime\prime\prime}. \tag{2.16}$$

The solution of the maximization problem subject to the constraints (2.15) and (2.16) can be obtained using the algorithm (referred to as **recolor1** from here on) given in Gunstensen's (1992) thesis. This algorithm leads to a maximum separation of the two fluids, but generates velocity fluctuations even for a non-inclined plain interface. An extensive discussion of spurious currents can be found in Ginzbourg (1994). We use a modified algorithm **recolor2**, which does not generate any velocity fluctuation for a plain interface. The separation of phases is not as strong as in algorithm **recolor1**, but the stability of the method is improved. Note that the choice of the recolouring algorithm does not alter the value of surface tension.

Algorithm 1. Recolouring algorithm 2.

```
procedure recolor2
  do a = 1, 17, 2 /* lattice vectors are sorted in antiparallel pairs */
    sp = e[a] · C
    tmp = sp * (1/|C|) * min(f^b[a], f^b[a + 1], f^r[a], f^r[a + 1])
    f^r[a] = f^r[a] + tmp
    f^r[a + 1] = f^r[a + 1] − tmp
    f^b[a] = f^b[a] − tmp
    f^b[a + 1] = f^b[a + 1] + tmp
  enddo
```

A more detailed description of the three-dimensional multicomponent code (e.g. data structures, vectorization and parallelization) can be found in Schulz (2001).

3. Verification

(a) Plain interface

As a first test we simulated a plain interface with a periodic system of size $2 \times 2 \times 32$. Parameters used are $\rho^{\mathrm{r}} = \rho^{\mathrm{b}} = 1.0$, $\alpha^{\mathrm{r}} = \alpha^{\mathrm{b}} = 0.2$, $\tau^{\mathrm{r}} = \tau^{\mathrm{b}} = 1.0$ and $A = 0.0004$. In figure 1 the resulting density profiles using algorithm 1 (part (*a*)) and algorithm 2 (part (*b*)) for the recolouring step are shown. The thickness of the interface is only

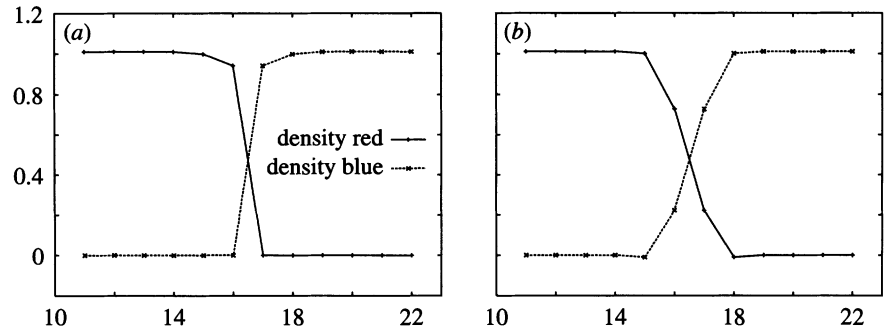

Figure 1. Density profile using (*a*) algorithm 1 and (*b*) algorithm 2.

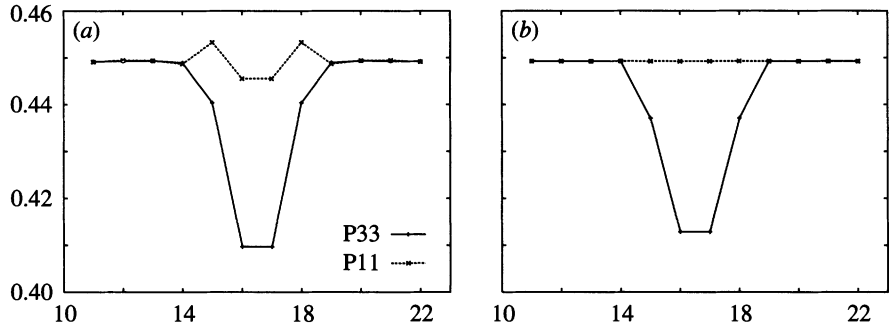

Figure 2. Components of the pressure tensor using (*a*) algorithm 1 and (*b*) algorithm 2.

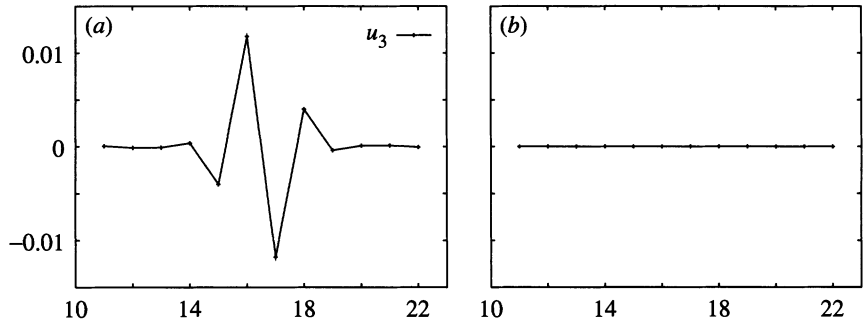

Figure 3. Velocity u_3 using (*a*) algorithm 1 and (*b*) algorithm 2.

one lattice spacing in the first case, whereas for the second case the thickness is about three lattice spacings. In figures 2 and 3, components of the pressure tensor and the velocity u_3 are shown. Note that algorithm 1 generates fluctuations in the pressure tensor as well as in the velocity even in this simple case of a plain interface.

(*b*) *Channel flow of two immiscible fluids*

The system consists of two immiscible fluids in a periodic channel subject to uniform body force parallel to the walls. The value of the surface tension is set to be zero. The analytical solution of the problem can be found in Ginzbourg (1994). The system size is $4 \times 4 \times 64$. Three tests with viscosity ratios of 4, 20 and 100 were

Table 1. *Bubble test on a* $65 \times 65 \times 65$ *grid*

ρ_b	ρ_r	α_b	α_r	A	σ_{theory}	σ_{Laplace}	relative error
1.0	1.0	$\frac{1}{5}$	$\frac{1}{5}$	1×10^{-4}	0.0240	0.0237	0.013
1.0	1.0	$\frac{1}{5}$	$\frac{1}{5}$	4×10^{-4}	0.0960	0.0956	0.004
1.0	1.0	$\frac{1}{5}$	$\frac{1}{5}$	1×10^{-3}	0.2400	0.2240	0.066
1.0	2.0	$\frac{1}{5}$	$\frac{3}{5}$	3×10^{-4}	0.1080	0.1067	0.012
1.0	10.0	$\frac{1}{5}$	$\frac{23}{25}$	1×10^{-4}	0.1320	0.1264	0.042
1.0	30.0	$\frac{1}{5}$	$\frac{73}{75}$	3×10^{-5}	0.1116	0.0966	0.134

conducted. The relative error in the maximum velocity was 1%, 4% and 6% for the three cases.

(*c*) *Test of Laplace's law with a single bubble*

The next test problem is a static spherical bubble of blue fluid immersed in the red fluid. The pressure jump Δp is given by Laplace's law:

$$\sigma = \tfrac{1}{2}\Delta p R. \tag{3.1}$$

Given the radius and the pressure jump from the simulation, one can compute the surface tension σ_{Laplace} using equation (3.1) and compare it with the value σ_{theory} using equation (2.13). The simulations were done on a 65^3 grid using periodic boundary conditions in all directions. The radius of the sphere was *ca.* 16 lattice units. In table 1 results for simulations with different values of surface tension and density ratios are given. The relaxation time τ was set to unity. Numerical results agree well with the theoretical ones. The results also indicate that the error increases as the surface tension or the density ratio increase.

(*d*) *Rise of a single bubble*

Extensive theoretical and experimental work on rising bubbles is found in the books of Clift *et al.* (1978) and Zapryanov & Tabakova (1999). In the case of a free rising bubble in an infinite medium, the bubble motion can be characterized by the viscosity ratio γ, the Eötvös number Eo, the Morton number Mo and the Reynolds number Re (Clift *et al.* 1978):

$$\gamma = \frac{\mu_i}{\mu}, \qquad Eo = \frac{g\Delta\rho d^2}{\sigma}, \qquad Mo = \frac{g\mu^4\Delta\rho d^2}{\rho^2\sigma^3}, \qquad Re = \frac{U_T d\rho}{\mu}, \tag{3.2}$$

where μ_i and μ are the dynamic viscosity of the inner and outer phase, $\Delta\rho$ is the density difference, d is the sphere diameter, ρ is the density of the outer phase, U_T is the terminal velocity, and g is the acceleration due to gravity. The shape of the bubble can be spherical, ellipsoidal, 'skirted', 'dimpled' or a 'spherical cap', depending on these parameters.

Table 2. *Simulation of a rising bubble in the spherical regime*

grid	ρ_b	ρ_r	D	σ	Eo	Mo	Re	U_t^{wall}	U_{num}	error
(a)	0.5	2	64	0.02	1.0	8.7×10^{-3}	0.27	0.0015	0.0014	0.07
(b)	0.5	2	128	0.02	1.0	8.7×10^{-3}	0.53	0.0030	0.0029	0.03

Table 3. *Simulation of a gas bubble (spherical cap regime)*

grid	ρ_b	ρ_r	D	σ	Eo	Mo	Re	U_t^W	U_{num}	error
(a)	0.5	2	64	1.2×10^{-4}	1462	348×10^3	3.06	0.017	0.015	0.12
(b)	0.5	2	129	1.2×10^{-4}	1462	348×10^3	3.87	0.022	0.024	0.09

(*e*) *Spherical regime*

For spherical bubbles with $Re < 1$ rising in a pipe, the terminal velocity can be approximated by the following solution (Clift *et al.* 1978)

$$U_t^W = \frac{1}{6}\frac{gd^2\Delta\rho}{\mu}\frac{\gamma+1}{3\gamma+2}\frac{1}{K}, \tag{3.3}$$

$$K = \frac{1 + 2.2757\lambda^5[(1-\gamma)/(2+3\gamma)]}{1 - 0.7017[(2+3\gamma)/(1+\gamma)]\lambda + 2.0865[\gamma/(1+\gamma)]\lambda^3 + 0.5689[(2-3\gamma)/(1+\gamma)]\lambda^5 - 0.726\,03[(1-\gamma)/(1+\gamma)]\lambda^6}, \tag{3.4}$$

where $\lambda = d/D$ is the ratio of the diameters of the sphere (d) and of the cylinder (D). In table 2 the results are given for the simulation of a rising bubble with $Re < 1$, $\nu = \frac{1}{6}$, $g = 1.5 \times 10^{-5}$ and $d = 30$ using (a) $65 \times 65 \times 513$ grids and (b) $129 \times 129 \times 513$ grids. Here U_t^W is the value computed from formula (3.3) and U_{num} is the simulation result.

(*f*) *'Dimpled' regime*

The terminal velocity for a bubble with $Eo > 40$ and $Mo > 200$ in an infinite medium satisfies the following equation (Clift *et al.* 1978):

$$2Re^2 + 6Re\frac{2+3\gamma}{1+\gamma} - Eo^{3/2}Mo^{-1/2} = 0. \tag{3.5}$$

The following empirical formula from Wallis (1969) takes into account the influence of the walls:

$$\frac{U_t^W}{U_t} = 1.13\exp\left(-\frac{d}{D}\right), \quad \frac{d}{D} < 0.6. \tag{3.6}$$

In table 3 the parameters and results for the simulation of a rising bubble using (a) $65 \times 65 \times 513$ grids and (b) $129 \times 129 \times 513$ grids are given ($g = 1.3 \times 10^{-4}$, $\nu = \frac{1}{6}$ and $d = 30$). The shape and the velocity with respect to a coordinate system moving with terminal velocity U_{num} are shown in figure 4.

The results in both cases (*e*) and (*f*) agree very well with the theoretical predictions.

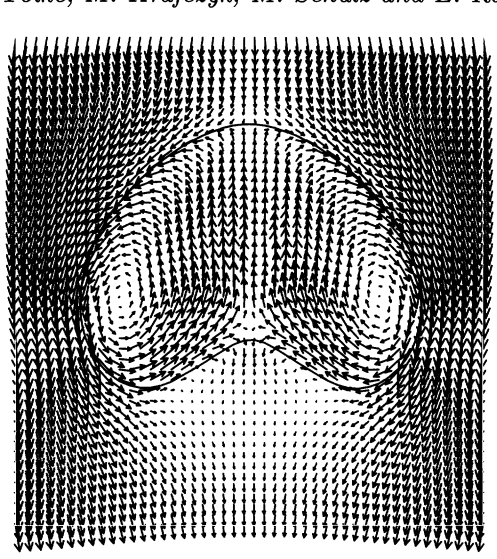

Figure 4. Shape and velocity field of a bubble in the 'dimpled'–regime.

4. Preliminary applications

(a) *Air-water flow in a laboratory-scale waste-water batch reactor*

In the field of waste-water treatment research a lot of laboratory-scale biofilm reactors are operated to better understand the relevant processes and, as a long-term goal, to optimize a real-world plant by an upscaling of the results obtained. One important phase of operation is the aeration of the bioreactor, where air bubbles are induced to activate certain biological processes. One important goal is to optimize the spatio-temporal homogeneity of nutrients and oxygen with respect to carrier body-size distribution, reactor shape and/or inflow nozzle geometry. The dynamics of this two-component system is completely determined by the geometric configuration of the flow, the inflow boundary conditions, the wetting properties of the media, and the following set of dimensionless parameters.

(1) Reynolds number: $Re = U_{\mathrm{m}} D/\nu$, where U_{m} is the mean flow velocity, D is the diameter of a typical carrier body, and ν is the kinematic viscosity of water.

(2) Weber number: $We = U_0^2 L\rho/\sigma$, where U_0 is the mean velocity of air bubbles, L their typical diameter, ρ the density of water, and σ the surface tension.

(3) The viscosity and density ratios of the two phases.

An estimation for these parameters for a typical laboratory-scale reactor is given in table 4. The geometric configuration is obtained from polydisperse sphere packings generated by molecular-dynamics-type simulations (Ristow 1994). Figure 5 gives an impression of the transient dynamics in the system including coalescence and breaking of bubbles. The modelled reactor contains *ca.* 600 spheres and 36 air nozzles at the bottom. The system is discretized by a $101 \times 101 \times 245$ grid. The dimensionless parameters are given in table 4 and differ by about one order of magnitude to those of the real-world system. The simulation captures important features observed in the experiment, e.g. an increased permeability close to the cylinder walls and the

Table 4. *Parameters for the real laboratory-scale reactor and the simulation*

	ρ_r/ρ_b	μ_r/μ_b	*Re*	*We*
simulation	4	4	*ca.* 3.5	*ca.* 0.1
laboratory scale reactor	850	40	*ca.* 20	*ca.* 0.01

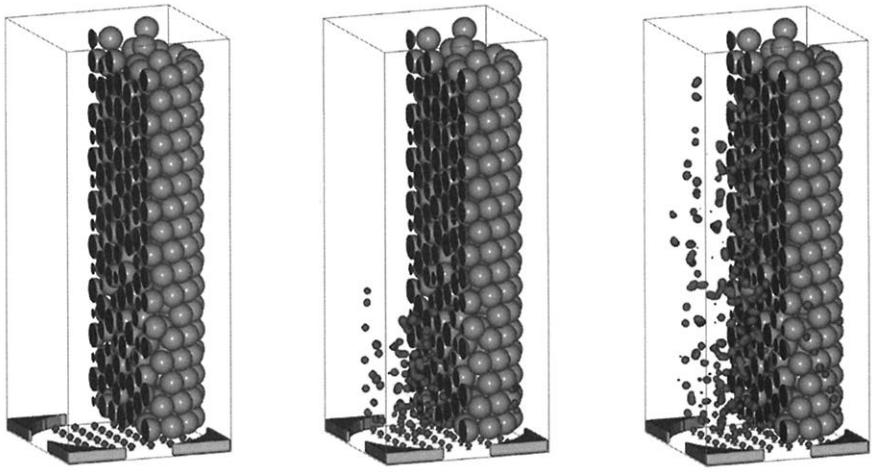

Figure 5. Spatio-temporal evolution of air bubbles in a model bioreactor sphere packing.

existence of preferential flow paths for the bubbles. The simulation time of 210 000 time-steps was sufficient to reach a steady state for quantities such as time-averaged spatial air concentration. A detailed discussion of the results is beyond the scope of this paper and can be found in Tölke (2001).

(*b*) *Hysteresis in air–water soil flow*

The reliable prediction of macroscopic air-water flow in soils, which is important for a variety of environmental problems, still remains as a challenging problem. One approach to improve the macroscopic modelling is to compute integral parameters such as (relative) permeabilities from simulated flow fields in a tomographically reproduced small specimen of soil. As water (in contrast to air) is soil wetting, the imbibition and drainage of microscopic soil samples induce hysteresis effects for the individual saturations and from such a hysteresis valuable information can be extracted for large-scale models which do not need the detailed pore structure anymore. Figure 6 shows a qualitative agreement between simulation and experiment for a soil probe discretized by 50^3 grid points.

Although we regard this preliminary result as encouraging, a convergence study with respect to grid refinement remains to be done and is the subject of future investigation. The computation of relative permeabilities in such geometries is much more difficult and poses severe stability problems for the model under consideration. To illustrate this, we note that the typical capillary number $\mathrm{Ca} = \rho\nu u_0/\sigma$ for soil is of the order of $O(10^{-5}$–$10^{-8})$, i.e. the dynamics is strongly dominated by capillary forces. For the Rothman–Keller-type LBGK model used here, one finds a stability limit of the form $\rho\nu/\sigma \simeq 1$, because there is an upper bound for the attainable

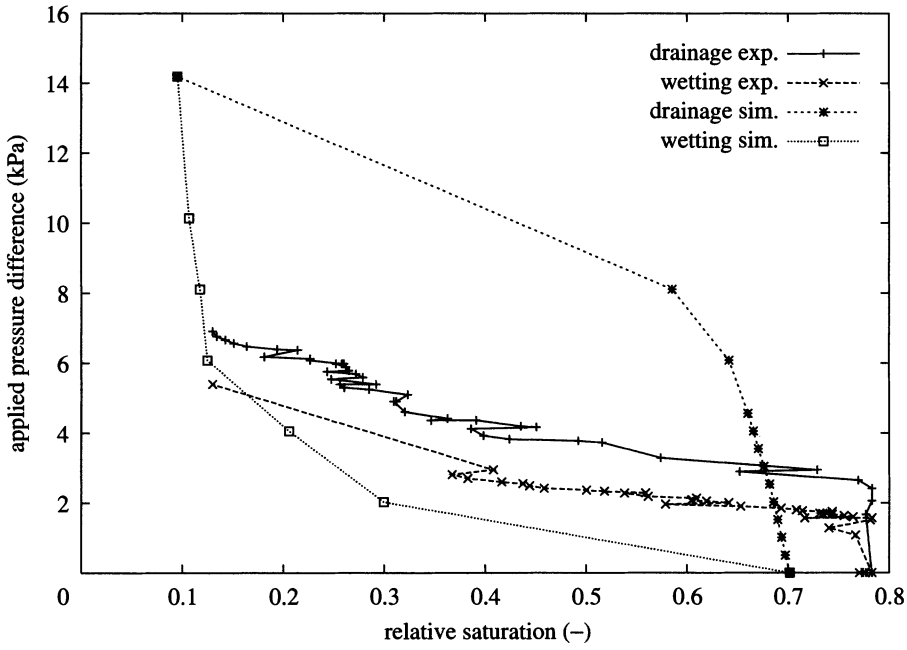

Figure 6. Experimental (Lehmann 1998) and simulated hysteresis curve after successive imbibition and drainage.

surface tension value, and for a given value of σ there is a lower bound for ν (i.e. τ). Simulating vanishing capillary numbers implies flow velocities u_0 of the order of Ca which would result in unbearable computation times. Thus we are faced with severe stability limitations, *even for a very low* Reynolds number. A potential remedy is probably the use of multiple relaxation time models which drastically improve the numerical stability (Ginzbourg 2001). We have not yet investigated the suitability of multicomponent LBGK models based on a van der Waals–Cahn–Hillard free-energy approach (Swift *et al.* 1995), but a recent study of bubble flow based on this approach (Takada *et al.* 2000) does not indicate significant advantages over the model used in this work.

5. Conclusions

In this work we show that the Rothman–Keller-type LBGK model for immiscible binary mixtures can be used to obtain quantitative results in the simulations of realistic problems of complex flows through porous media. However, for the simulations of large-scale problems in reality, the stability constraints seem to pose a major limitation. Therefore, whether LBGK models are the most suitable ones to solve these difficult problems remains an open question to the authors. With these concerns in mind, one should exercise certain caution when promoting the LBGK-type model as an efficient simulation tool for complex flows through porous media. We believe, that the lattice Boltzmann model used in this work still needs qualitative improvement before it can be used in realistic applications. Yet, we would also like to point out that, to the best of our knowledge, there is no traditional Navier–Stokes solver which

is *a priori* superior to the lattice Boltzmann equation for these challenging problems of complex fluid flows.

The authors thank the unknown referee and Dr Li-Shi Luo for valuable suggestions and comments.

References

Bhatnagar, P. L., Gross, E. P. & Krook, M. 1954 A model for collision processes in gases. I. Small amplitude processes in charged and neutral one-component systems. *Phys. Rev.* **94**, 511–525.

Chen, S. & Doolen, G. 1998 *A. Rev. Fluid Mech.* **30**, 329.

Clift, R., Grace, J. R. & Weber, M. E. 1978 *Bubbles, drops and particles.* Academic.

Ginzbourg, I. 1994 Les probèmes des conditions aux limites dans les méthodes de gaz sur réseaux à plusieurs phases. PhD thesis, Université de Paris 6, Paris.

Ginzbourg, I. 2001 Introduction of upwind and free boundary into the lattice Boltzmann method. In *Discrete modelling and discrete algorithms in continuum mechanics* (ed. Th. Sonar & I. Thomas), pp. 97–110. Berlin: Logos.

Ginzbourg, I. & Adler, P. M. 1995 Surface tension models with different viscosities. *Transport Porous Media* **20**, 37.

Grunau, D., Chen, S. & Eggert, K. 1993 A lattice Boltzmann model for multiphase flow. *Phys. Fluids* A **5**, 2557–2561.

Gunstensen, A. K. 1992 Lattice Boltzmann studies of multiphase flow through porous media. PhD thesis, Massachusetts Institute of Technology, Boston, MA.

Gunstensen, A. K. & Rothman, D. 1991 Lattice Boltzmann model of immiscible fluids. *Phys. Rev.* A **43**, 4320–4327.

Lehmann, P., Stauffer, F., Hinz, C., Drury, O. & Flühler, H. 1998 Effect of hysteresis on water flow in a sand column with a fluctuating capillary fringe. *J. Contaminant Hydrol.* **33**, 81–100.

Ristow, G. H. 1994 Granular dynamics: a review about recent molecular dynamics simulations of granular materials. *A. Rev. Computat. Phys.* **1**, 275–308.

Rothman, D. H. & Keller, J. M. 1988 Immiscible cellular automaton fluids. *J. Stat. Phys.* **52**, 1119–1127.

Schelkle, M. 1996 LB-Verfahren zur Simulation dreidimensionaler Zweiphasen-Strömungen mit freien Oberflächen. PhD thesis, Universität zu Stuttgart, Stuttgart.

Schulz, M., Krafczyk, M., Tölke, J. & Rank, E. 2001 Parallelization strategies and efficiency of CFD computations in geometries using lattice Boltzmann methods on high-performance computers. Preprint.

Shan, X. & Chen, H. 1993 Lattice Boltzmann model for simulating flows with multiple phases and components. *Phys. Rev.* E **47**, 1815–1819.

Swift, M. R., Osborn, W. R. & Yeomans, J. M. 1995 Lattice Boltzmann simulation of nonideal fluids. *Phys. Rev. Lett.* **75**, 830.

Takada, M., Misawa, M., Tomiyama, A. & Fujiwara, S. 2000 Numerical simulation of two- and three-dimensional two-phase fluid motion by lattice Boltzmann method. *Comput. Phys. Commun.* **129**, 233–246.

Tölke, J. 2001 Gitter–Boltzmann–Verfahren zur Simulation von Zweiphasenströmungen. PhD thesis, Lehrstuhl Bauinformatik, TU München, München.

Wallis, G. B. 1969 *One-dimensional two-phase flow.* McGraw-Hill.

Zapryanov, Z. & Tabakova, S. 1999 *Dynamics of bubbles, drops and rigid particles.* Dordrecht: Kluwer.